A theoretical study of the effect of a non-aqueous proton donor on electrochemical ammonia synthesis

Linan Zhang,[ab] Shaama Mallikarjun Sharada,[bcd] Aayush R. Singh,[c] Brian A. Rohr,[c] Yanjing Su,[a] Lijie Qiao,[a] and Jens K. Nørskov[*bc]

[a]Corrosion and Protection Center, Key Laboratory for Environmental Fracture (MOE), University of Science and Technology Beijing, Beijing, 100083, China

[b]SUNCAT Center for Interface Science and Catalysis, SLAC National Accelerator Laboratory, Menlo Park, CA, 94025, USA

[c]SUNCAT Center for Interface Science and Catalysis, Department of Chemical Engineering, Stanford University, Stanford, CA, 94305, USA

[d]Mork Family Department of Chemical Engineering and Materials Science, University of Southern California, Los Angeles, CA 90089-1211, USA

E-mail: norskov@stanford.edu

Abstract

Ammonia synthesis is one of the most studied reactions in heterogeneous catalysis. To date, however, electrochemical N_2 reduction in aqueous systems has proven to be extremely difficult, mainly due to the competing hydrogen evolution reaction (HER). Recently, it has been shown that transition metal complexes based on molybdenum can reduce N_2 to ammonia at room temperature and ambient pressure in a non-aqueous system, with a relatively small amount of hydrogen output. We demonstrate that the non-aqueous proton donor they have chosen, 2,6-lutidinium ($LutH^+$), is a viable substitute for hydronium in the electrochemical process at a solid surface, since this donor can suppress the HER rate. We also show that the presence of $LutH^+$ can selectively stabilize the *NNH intermediate relative to *NH or *NH_2 via formation of hydrogen bonds, indicating that the use of non-aqueous solvents can break the scaling relationship between limiting potential and binding energies.

Introduction

The abundant nitrogen resources in the atmosphere can only be used biologically in the form of ammonia or products derived from it[1]. The conversion of nitrogen to ammonia for fertilizer production has played a critical role in the growth and sustenance of the world's population[2]. Furthermore, as a carbon-free and high-energy density liquid fuel[3], ammonia can be a potential substitute for traditional fossil fuels in the near future.

In industry, ammonia is produced using gas phase N_2 and H_2 by the Haber-Bosch process[4] at high temperature (approximately 400 °C) and pressure (100-150 bar) over Fe[5, 6] or Ru[7-10] catalytic particles, in order to activate the strong N-N triple bond. This is an energy-intensive process[11], relying mostly on fossil fuel as not only the energy source, but also a chemical feedstock. Almost all of the hydrogen gas used for ammonia synthesis is produced by steam reforming of methane, which is energy intensive and unsustainable[12]. From an environmental point of view, if other hydrogen sources without reforming or decomposition steps could be chosen, it would be much more favorable[13].

In contrast, nature has developed a route for N_2 conversion under ambient conditions. While the Haber-Bosch process proceeds via a dissociative reduction mechanism[14], the nitrogenase enzyme catalytically weakens the N-N bond through successive proton-electron transfers, referred to as the associative mechanism[15-17]. The biological process is quite inefficient since 16 ATP per reduced N_2 is required, the hydrolysis of which is needed to increase the chemical potential of electrons, corresponding to an energy expense of ~5 eV per turnover of one N_2 molecule[18]. It is conceivable that this natural process can be emulated in an electrochemical cell with lower energy consumption than the current industrial process[19, 20], where the protons can come from water splitting, the electrons can be driven to the interface by an applied bias and renewable energy resources like wind or solar power can be used instead of fossil fuels.

The main challenge with this electrochemical reaction is the poor selectivity towards reduction of N_2 to ammonia. Few electrochemical systems that produce large quantities of ammonia with high Faradaic Efficiencies (0.1 mA/cm^2 at 10% FE) have been reported to date, mainly due to competition with the hydrogen evolution reaction (HER)[21, 22]. The problem with selectivity for heterogeneous surfaces is related to the fact that the surfaces covered by H can catalyze HER at low overpotentials[20]. Montoya *et al*.[23] have demonstrated that the potential required to drive the N_2 reduction, even for the best transition metal catalysts, is quite negative (at least -1V). Under such cathodic potentials, most surfaces will be fully covered with H adatoms, thereby lowering the possibility of *NNH (the first and a key reduction product of N_2) formation[24]. Hence, the selectivity towards NH_3 becomes negligible, and H_2 becomes the dominant product.

Recently, numerous experimental and theoretical studies have been focused on the electrochemical synthesis of ammonia and they have provided excellent insights into the

development of new reaction and catalytic resources for this reaction. Transition metal nitrides are widely used, on which the production of ammonia is predicted to occur at smaller overpotentials. The competing reaction, HER, then can be suppressed as the reaction can proceed via the Mars-van Krevelen mechanism[25], in which a surface N atom is reduced to NH_3 and the generated nitrogen vacancy is then replenished with gaseous N_2. Co_3Mo_3N is one of the most active catalysts for ammonia synthesis, on which it is demonstrated that the Mars-van Krevelen mechanism dominates compared to associative or dissociative mechanism[26]. VN, ZrN, NbN, CrN and RuN are promising candidates, on the single-crystal facets of which N_2 reduction can be catalyzed in high yield at low onset potentials[27, 28]. While in practice, polycrystalline surfaces would always be used. As other facets of these nitrides are taken into account, ZrN is the only probable candidate, for all its facets would be active and stable for ammonia synthesis under operating conditions and would not decompose[29, 30]. Some theoretical studies indicate that transition metal nanoclusters can also be active catalysts for both associative and dissociative N_2 reduction[14, 31].

Yandulov and Schrock[32] have accomplished a successful formation of ammonia (67% yield of ammonia was obtained) on transition metal complexes based on molybdenum at room temperature and ambient pressure. Unlike using the aqueous system, dinitrogen is reduced catalytically in heptane with 2,6-lutidinium as the proton source and decamethylchromocene [$Cr(\eta^5\text{-}C_5Me_5)_2$, or $CrCp^*_2$] as the reducing agent[33-36]. It has been shown theoretically[37] that the overall mechanism of the Schrock Cycle appears to be quite similar to that of the nitrogenase reaction. In the Schrock process, the formation of hydrogen gas can be largely suppressed by dropwise addition of the reducing agent, in association with the poorly soluble acid[32]. It has been demonstrated by Singh *et al.*[38] that lowering the accessibility of electrons, protons or both can increase the NH_3 selectivity in any system, homogeneous or heterogeneous.

In this work, we present a theoretical study of associative electrochemical ammonia synthesis over close-packed transition metal surfaces using a non-aqueous proton source, 2,6-lutidinium ($LutH^+$), which has been chosen in the Schrock Cycle[32]. We first show that the competing hydrogen evolution reaction (HER) can be suppressed relative to hydronium as proton donor. The Volmer reaction has a significantly higher barrier with $LutH^+$ as proton donor species when compared with hydronium, thereby lowering the probability of occurrence of the Heyrovky reaction, or HER. Secondly, we examine the configuration and stability of intermediates ($*NNH_x$ (x = 0, 1, 2) and $*NH_x$ (x = 0, 1, 2)) in the N_2 reduction system. Co-adsorption with $LutH^+$ can selectively stabilize the $*NNH_x$ species through formation of hydrogen bonds while destabilize $*NH_x$ species, giving rise to a smaller limiting potential for electrochemical N_2 reduction. As a result, we conclude that such non-aqueous systems may be much more selective for ammonia synthesis.

Computational Method

Density functional theory

All calculations are carried out using the Quantum Espresso software package[39], interfaced with the Atomic Simulation Environment (ASE)[40]. The BEEF-vdW[41] exchange correlation functional is selected for its accurate estimation of adsorption energies[42] and its consideration of the van der Waals interactions. A Fermi-Dirac smearing of 0.1 eV is applied. Plane wave basis sets with kinetic energies up to 500 eV are used. The k-points are sampled using a 3×3×1 Monkhorst-Pack grid[43]. The difference in adsorption energies between this value and a denser k-points sampling, 4×4×1, is found to be less than 0.01 eV according to a few tests.

Simulations are carried out on close-packed face-centered cubic (fcc) surfaces with optimized metal lattice constants (see supporting information, Table S1). All surfaces are modeled by periodically repeated 4×4 three layer slabs. The slabs are separated by at least 15 Å of vacuum in the z-direction of the interface. The two bottom metal layers are fixed, while the topmost layer and the adsorbates are geometrically relaxed so that the maximum force in any direction on any moveable atom is less than 0.03 eV/Å. Dipole correction is included in all cases to decouple the electrostatic interaction between periodically repeated slabs.

Electrochemical treatment

We calculate the reaction barriers to the Volmer reaction[44] and the Heyrovsky reaction[45] using the non-aqueous proton donor, $LutH^+$, on a series of flat transition metal surfaces, which are then compared with the aqueous results. The NEB (nudged elastic band)[46] method is used to calculate transition state geometries, and all of the transition states have been verified by their vibrational frequencies.

Volmer reaction:

$$LutH^+ + e^- \rightleftharpoons Lut + *H \quad (1)$$

$$H_3O^+ + e^- \rightleftharpoons H_2O + *H \quad (2)$$

which corresponds to a proton transferred from the proton donor to the surface. An asterisk, *, denotes an adsorption site on the surface.

Heyrovsky reaction:

$$LutH^+ + *H + e^- \rightleftharpoons Lut + H_2(g) \quad (3)$$

$$H_3O^+ + *H + e^- \rightleftharpoons H_2O + H_2(g) \quad (4)$$

a proton from the proton donor will attach to an H^--like species on the surface to form an H_2 molecule without first adsorbing on the surface (compared with Tafel reaction[47]).

To analyze the energetics of elementary steps involving a proton-coupled electron transfer, we use the computational hydrogen electrode[48] (CHE). By choosing standard hydrogen electrode (SHE) as the reference state, the chemical potential of the

proton-electron pair is related to that of one-half hydrogen:

$$\frac{1}{2}H_2(g) \rightleftharpoons H^+ + e^- \quad (5)$$

Real electrochemical reactions are always operated at constant potential. On the other hand, DFT simulations of electrochemical barriers are typically performed at constant charge, as a result of which interfacial charge density and the corresponding potential will change along the reaction path[49, 50]. One way to overcome this issue is to increase the size of unit cell[24,51] until the interfacial charge density change during a charge transfer reaction from initial state to final state becomes negligible. However, a larger unit cell is computationally demanding. An efficient alternative is to use an approximate charge extrapolation method proposed by Chan *et al*.[52] For a given interfacial charge transfer process, the chemical and electrostatic contributions to the change in energy are separable. For simple proton transfers, the electrostatic component is purely capacitive. With surface charge density, the capacitance and capacitor energy per surface atom can be determined. According to this method, the total energy change from state 1 to 2 at a constant potential Φ_1 can be decided by:

$$E_2(\Phi_1) - E_1(\Phi_1) = E_2(\Phi_2) - E_1(\Phi_1) + (q_2-q_1)(\Phi_2-\Phi_1)/2 \quad (6)$$

where $E_2(\Phi_2)-E_1(\Phi_1)$ and $\Phi_2-\Phi_1$ are the DFT-based reaction energy change and work function change, respectively. q_2-q_1 represents the change in surface charge from state 1 to 2, estimated using Bader Analysis[53]. This simple method is applicable to both reaction energy (ΔE) and activation energy (E_a), which has been used to determine the kinetics of HER in this work. All the barriers hereinafter are extrapolated to U = 0 V (vs. SHE).

We then investigate the configurations and binding energies for all the reaction intermediates (*NNH_x (x =0, 1, 2) and *NH_x (x = 0, 1, 2)) in the electrochemical reduction of N_2 on a few fcc(111) surfaces. Several structures and adsorption sites are tested in each case. By using standard vibrational corrections within the harmonic oscillator approach and a frozen slab approximation, we calculate the vibrational frequencies for all the intermediates. From the vibrational frequencies, zero-point energy (ZPE) corrections are included and the entropy and enthalpy under reaction conditions are determined. The change in free energy is given by:

$$\Delta G = \Delta E + \Delta E_{ZPE} - T\Delta S \quad (7)$$

where ΔE is the reaction energy of each intermediate step, ΔE_{ZPE} is the zero-point energy correction and $T\Delta S$ is the entropy change under a certain temperature. Referenced to gaseous N_2 and H_2, the free binding energies for all the intermediates can be determined.

Results and discussion

Adsorption of 2,6-lutidinium on transition metal surfaces

We have compared two orientations of 2,6-lutidinium ($LutH^+$) adsorbed on Pt(111), shown in Figure 1. The parallel configuration of $LutH^+$ binds stronger to the surface by 0.18 eV relative to the perpendicular one, leading us to conclude that the binding of the species is dominated by electrostatic interactions. Therefore, the parallel configuration is adopted in all of our calculations.

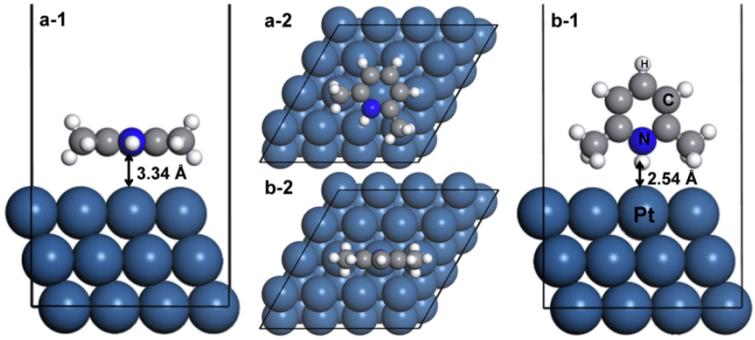

Figure 1 2,6-lutidinium adsorption configurations on Pt(111) - (a) parallel to the surface (b) perpendicular to the surface. (1) indicates side view and (2) is the top view. The solid line represents the size of one unit cell.

The calculated binding energies (E_b) of $LutH^+$ on different transition metal terraces are shown in Table 1. Although the equilibrium height of $LutH^+$ exceeds 3 Å, binding is favorable, largely due to the electrostatic interactions, which are accurately captured by the BEEF-vdW functional[41]. It is worth noting that the binding on Pt(111) is significantly stronger than the remaining surfaces.

Table 1 Binding energies (E_b) of $LutH^+$ adsorbed on different fcc(111) metal surfaces. d refers to the average vertical distance between the H^+ of $LutH^+$ and the first layer of the metal surface.

	Ag(111)	Cu(111)	Ir(111)	Pd(111)	Pt(111)	Re(111)	Rh(111)	Ru(111)
E_b /eV	-0.36	-0.46	-1.00	-1.03	-1.48	-0.69	-0.86	-0.87
d /Å	3.77	3.76	3.60	3.40	3.43	3.73	3.61	3.63

In order to understand these trends, we determine the relationship between the binding energy of $LutH^+$ and work function of the clean transition metal surface, shown in Figure 2. As the clean Pt(111) has a relatively large work function, it can become more stable upon transferring an electron. Therefore, the $LutH^+$ binds stronger on Pt(111).

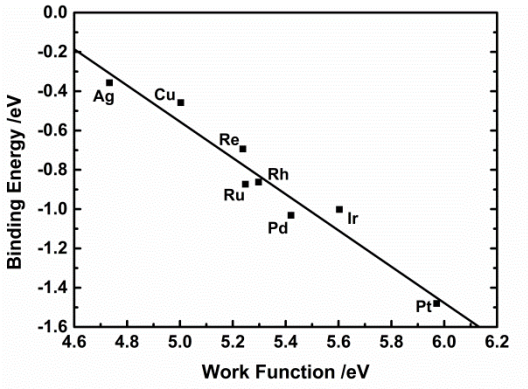

Figure 2 Relationship between the binding energies of $LutH^+$ adsorbed on transition metal (111) surfaces and the work functions of the corresponding clean surface.

The projected density of states (PDOS) for the adsorbed $LutH^+$ on these surfaces, shown in Figure 3, further illustrates this point. We focus only on the N atom of $LutH^+$ and the proton adjacent to it, as well as the surface atom. Here we choose Ru (more reactive than Pt) and Ag (less reactive than Pt) as representatives to be compared with Pt. The filling of the antibonding states of N on other metal surfaces are similar with Ru and Ag. In the d-band model[54] the electronic states of transition metal surfaces are divided into 2 types: the sp-bands and d-bands. When the $LutH^+$ approaches the surface, we have an empty H_{1s} state well above the Fermi level (shown in red) and bonding states are formed between the metal sp-states (shown in green) and the N 2p states. As all transition metals have similar broad sp-bands, the bond energy contribution from the sp-electrons is large and independent of the metal. Then the renormalized N 2p states couples with the metal d-states (shown in blue) to form bonding and antibonding states (shown in magenta). This gives rise to further contributions to the bond energy and the strength of the interaction will depend on the filling of the antibonding states. At a metal surface, the filling depends on the position of the antibonding states relative to the Fermi level. On Pt(111), the antibonding states of the N atom is apparently less filled compared with on Ag(111) and Ru(111), which gives a further explanation for the stronger binding.

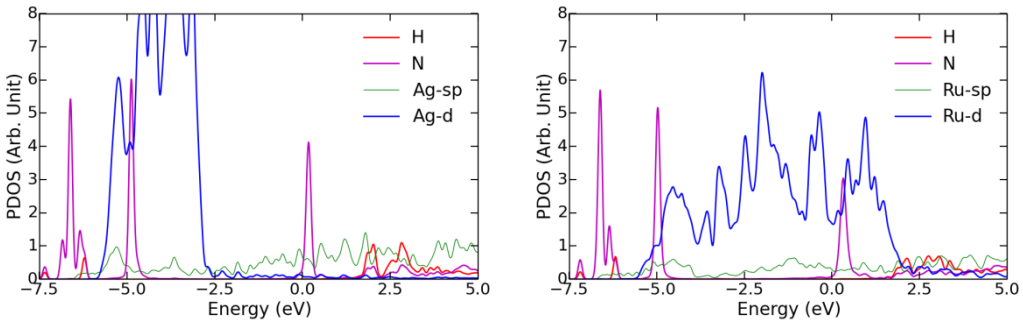

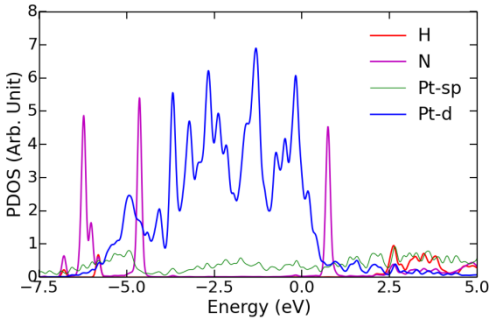

Figure 3 Projected density of states (PDOS) on N and H^+ adjacent to it, and also on surface metal atoms (Ag, Ru, Pt) for $LutH^+$ adsorption. See Figure 1(a) for the structure. The Fermi level corresponds to the origin of the energy-axis.

Hydrogen evolution reactions (HER)

The key problem faced by the electrochemical N_2 reduction is the competing hydrogen evolution reaction (HER). One possible solution is to prevent H adsorption on the surface by employing proton donors that preferentially donate protons to the adsorbed N-N species. We contrast the selectivity of the non-aqueous proton donor 2,6-lutidinium ($LutH^+$) to HER relative to the aqueous donor hydronium (H_3O^+).

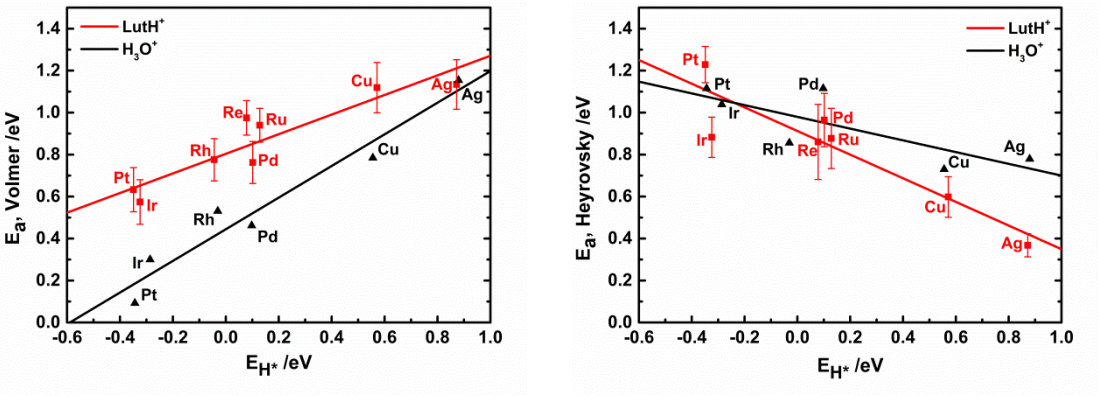

Figure 4 Scaling relation between reaction barriers (E_a) (left-Volmer, right-Heyrovsky) and H binding energies on the ontop-sites (E_{H^*}) of different flat transition metal surfaces. The black ones are results of H_3O^+ taken from Liu *et al*. (calculation details and error bars can be found in their supporting information)[55], while the red line and dots represent our results of $LutH^+$ with same functional and input parameters (see supporting information for the NEB profiles calculated for the original barriers, Figure S1). All these calculations are done at U = 0 V (SHE).

The catalytic activity for heterogeneous reactions occurring on transition metal surfaces can be interpolated and summarized using approximate linear relations between reaction/activation energies and adsorption energies[56, 57]. In Figure 4, the reaction barriers

scale well with the H binding energies. It should be pointed out that, the descriptor, namely the H binding energies, are all for H bound on the ontop-site of the metal surface, instead of on the most stable site (generally fcc-site). Although the H atom preferably adsorbs on the most stable site in the final state, in the transition state of the Volmer reaction, the H transferred from the proton donor (either from $LutH^+$ or H_3O^+) adsorbs on the top site first, followed by a hop to its final position. During the course of the Heyrovsky reaction, the pre-adsorbed H also tends to move to the neighboring top site before combining with the transferred proton to form H_2 gas. Therefore, the top site is a better-suited descriptor to determine barrier scaling.

For Volmer reaction, depicted on the left of Figure 4, weaker binding of H translates to a larger barrier for proton transfer. With the exception of Ag, the proton transfer barriers with the $LutH^+$ donor are significantly higher than those with hydronium. The most dramatic case is Pt(111), on which the Volmer reaction with H_3O^+ is almost barrierless (~0.1 eV), while the barrier is 0.6 eV with $LutH^+$. These results clearly indicate that it is much more difficult to transfer a proton to the surface using $LutH^+$ than using H_3O^+.

Since $LutH^+$ is a relatively weak acid (pKa in water = 6.75[35]), it does not donate a proton easily. During the proton transfer from $LutH^+$ to the surface, the metal lattice exhibits puckering. The metal atom accepting the proton is displaced by almost 0.3 Å, which may be energetically unfavorable. In contrast, the lattice distortion with H_3O^+ is rather small (~0.1 Å). The exception is Ag(111), on which the H-binding energy is quite positive (0.87 eV). The displacement of the metal atom caused by the weak H adsorption is negligible in both cases, resulting in similar barriers.

We further examine the proton transfer process using $LutH^+$ on transition metal surfaces by the projected density of states on H^+ next to the N atom of the $LutH^+$. The results for Cu(111) are shown in Figure 5. Although the transfers are quite similar using these two donors ($LutH^+$ and H_3O^+), the resulting PDOS plots are different. When using $LutH^+$, in the initial state (IS), as shown in the former part, we have an empty H_{1s} state. The energy peak is at around 2.5 eV. Then in the transition state (TS), the energy state moves down to the Fermi level (0 eV). Finally in the final state (FS), bonding states forms at ~ -7 eV. While for the water case, in the transition state, the energy state of the proton spreads broadly near the Fermi level (see supporting information, Figure S2), indicating it's much easier for the proton comes from the H_3O^+ to receive electrons from the surface, which may lead to lower barriers.

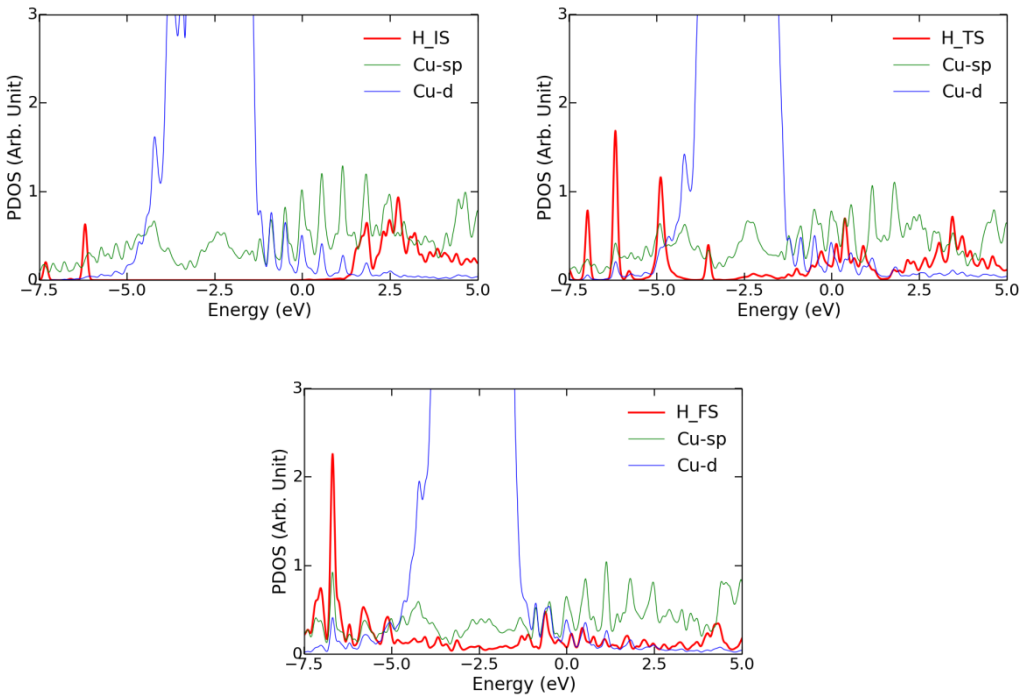

Figure 5 Projected density of states (PDOS) on H^+ adjacent to the N atom of $LutH^+$ and also the surface copper atoms for proton transferring from the $LutH^+$. See Figure 1(a) for the structure. IS, TS and FS corresponds to the initial state, transition state and final state, respectively. The Fermi level corresponds to the origin of the energy-axis.

In the Heyrovsky reaction, shown on the right of Figure 4, weaker H-binding energy corresponds to smaller desorption barrier. In marked contrast to the Volmer reaction, the barriers are very similar (with the exception of Ag) for both proton donors. On Ag(111), the pre-adsorbed H is rather easy to desorb, what counts for the H_3O^+ case is due to the explicit presence of water layer, it may be hard for the bound H (and H_2 gas) to go upward, leading to a larger barrier.

Therefore, the $LutH^+$ donor likely outperforms H_3O^+ in the suppression of HER, because the Volmer reaction is less favorable with $LutH^+$. And since the Volmer step must occur first, the subsequent Heyrovsky step on the transition metal surfaces can be avoided if another adsorbate can bind to the surface before an H atom. We then conclude that we can expect for better selective reduction of N_2 to ammonia using $LutH^+$ for the HER is suppressed.

Electrochemical N_2 reduction reaction (NRR)

The results above demonstrate that the difference in the Volmer barriers for the two proton donors ($LutH^+$ and H_3O^+) can mostly be attributed to the bulky solvent ($LutH^+$) not being able to get very close to the surface, resulting in surface puckering. The Heyrovsky step, on the other hand, does not change much with the solvent. The similarity between

the Heyrovsky barriers for $LutH^+$ and H_3O^+ indicates that hydrogenation of adsorbates on the surface (onto an H, an N_2, or other intermediates) does not require surface puckering and remains facile when $LutH^+$ is the solvent, which is the ideal scenario for electrochemical N_2 reduction. We expect, therefore, that the kinetics of proton transfer to nitrogen intermediates in both non-aqueous and aqueous systems will follow similar scaling behavior with respect to the thermodynamics of intermediates. In the following section, we consider how the thermodynamics of N_2 reduction are affected by the switch in solvent from H_3O^+ to $LutH^+$.

We construct the Gibbs free energy diagram for electrochemical N_2 reduction through successive proton-coupled electron transfer on Ru(111), a commonly used catalyst in the Haber-Bosch process, shown in Figure 6. It shows that the thermodynamic process of N_2 reduction is not very different with aqueous (shown in black) or non-aqueous (shown in red) proton donors. The overall reaction from nitrogen to the formation of ammonia on Ru(111) is exergonic. The most endergonic step is the addition of the first proton to the adsorbed N_2 molecule to form *NNH.

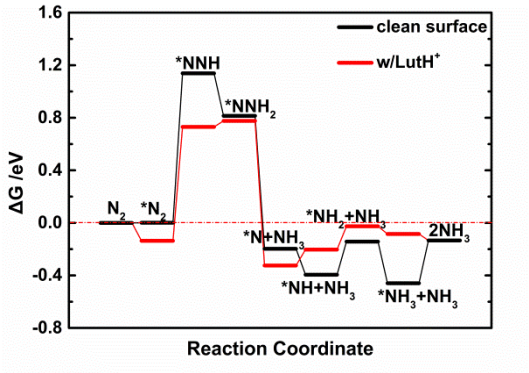

Figure 6 Free energy diagram for the associative reduction of N_2 on Ru(111) (black). The using of $LutH^+$ has been shown in red. Results are obtained from DFT calculations of the binding energies and vibrational frequencies, as well as entropy of the gas molecules. An asterisk, *, denotes an adsorption site on the surface.

However, the influence of co-adsorption with $LutH^+$ on the binding energies of intermediates is clearly depicted. In our model, as the $LutH^+$ is partially positive, the surface is negatively charged in order to keep the system neutral. Then an electrostatic field outside the surface can be set up. Owing to the field effect[58], the N_2 molecule possesses a small negative charge, and the interaction between the induced field and the molecular dipole moment becomes attractive. Moreover, the $LutH^+$ can further stabilize N_2 adsorption by forming a hydrogen bond. When compared with a clean surface, onto which the adsorption of N_2 from gas phase is endergonic, the lowering in free binding energy due to the presence of $LutH^+$ is sufficient to make the adsorption exergonic irrespective of the large entropy loss associated with surface adsorption. Similarly, we demonstrate the

presence of $LutH^+$ can stabilize $*NNH_x$ (x = 0, 1) species via formation of hydrogen bonds to the adsorbate but not to $*NH_x$ (x = 1, 2) species. The extent of the influence varies with transition metal, but the trends are similar.

As suggested by Montoya *et al.*[23], the challenge of the electrochemical reduction of N_2 to NH_3 is to design and synthesize a system that can achieve the requirements of selectively stabilizing *NNH and/or destabilizing $*NH_2$, which will lead to higher limiting potential (U_L). The negative of the free energy difference of an elementary step, $-\Delta G$, is defined as the limiting potential (U_L) -- the applied potential required such that the reaction downhill in free energy at each step. For surfaces like Ru(111), the potential-limiting step is the reductive adsorption of N_2 to form *NNH. When *NNH binds stronger to the surface, the reaction energy for this step, which corresponds to the negative value of U_L, will be lower. For Re(111), the limiting step is the reduction of *NH to form $*NH_2$ (see supporting information, Figure S3). When the adsorption of the $*NH_2$ is destabilized, it is much easier for the intermediate to desorb and hence free up more sites. Then the reaction energy should also be lower (higher U_L).

With the limiting potentials we obtain on each surface, we determine that all the values of the reductive N_2 adsorption step fall off the original scaling line of the clean surface, while the reduction of *NH step does not change significantly. The results are shown in Figure 7. In the presence of $LutH^+$, the maximum value of the limiting potential U_L can be shifted upwards by 0.3 V. On the other hand, in aqueous systems, the solvation effects may only raise the theoretical limiting potentials by up to 0.1 V[23].

Although the limiting potential we determine is still lower than that of the hydrogen evolution reaction[23], HER is successfully suppressed by high barriers to the Volmer reaction. Therefore, the 2,6-lutidinium can be a very promising candidate for electrochemical N_2 reduction.

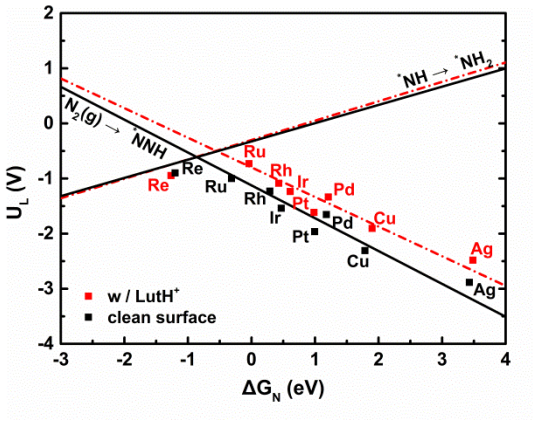

Figure 7 Limiting potentials (U_L) of N_2 electro-reduction as a function of N-binding energy (ΔG_N) for the fcc(111) terraces. For the most reactive surface, Re(111), the reduction is limited by the protonation of *NH to form $*NH_2$. For other surfaces, the limiting

step is the reductive adsorption of N_2 to form *NNH. The dots are DFT results. Color black represents calculations performed on clean surfaces, results taken from Montoya *et al*.[23] When in the presence of $LutH^+$, the results are shown in red.

Conclusions

We have compared the selectivity of a non-aqueous proton donor, 2,6-lutidinium ($LutH^+$), to the electrochemical N_2 reduction with that of the hydronium. We demonstrate that the competing HER process can be suppressed, since the Volmer reaction is rendered with quite higher barriers using $LutH^+$ when compared to H_3O^+, mainly due to surface puckering. As a result of which it is much more difficult to get H onto the surface. Then the hydrogen evolution step, the Heyrovky reaction, is prohibited. The similarity between the Heyrovsky barriers with the two proton donors indicates that the rates of hydrogenation of adsorbed N_2 and subsequent intermediates are still sufficiently fast. Therefore, a non-aqueous proton donor like $LutH^+$, is a very promising candidate for electrochemical N_2 reduction.

We also show that the thermodynamic process of N_2 reduction is not very different with aqueous or non-aqueous proton donors. By using $LutH^+$, we can achieve higher selectivity without affecting the limiting potential. In fact, the maximum value of the limiting potential can be shifted upwards by 0.3 V in the presence of $LutH^+$, while solvation effects in the aqueous system may only raise the limiting potentials by up to 0.1 V.

Acknowledgment

This work was supported by a research grant (9455) from VILLUM FONDEN. B.A.R. was supported by the NSF GFRP, grant number DGE-1656518. The authors gratefully acknowledge financial support from China Scholarship Council.

References

(1) V. Smil, *Enriching the earth: Fritz Haber, Carl Bosch, and the transformation of world food production*, MIT press, 2004.
(2) V. Smil, *Scientific American*, 1997, **277**, 76-81.
(3) A. Klerke, C. H. Christensen, J. K. Nørskov and T. Vegge, *Journal of Materials Chemistry*, 2008, **18**, 2285-2392.
(4) C. Bosch, *The Nobel Foundation. Nobel Lectures Including Presentation Speeches and Laureates' Biographies: Chemistry*, 1922, **1941**, 197-241.
(5) G. Ertl, S. Lee and M. Weiss, *Surface Science*, 1982, **114**, 527-545.
(6) S. R. Bare, D. Strongin and G. Somorjai, *The Journal of Physical Chemistry*, 1986, **90**, 4726-4729.
(7) K.-i. Aika, H. Hori and A. Ozaki, *Journal of Catalysis*, 1972, **27**, 424-431.

(8) S. Dahl, P. Taylor, E. Törnqvist and I. Chorkendorff, *Journal of Catalysis*, 1998, **178**, 679-686.
(9) Á. Logadóttir and J. K. Nørskov, *Journal of Catalysis*, 2003, **220**, 273-279.
(10) A. Hellman, E. Baerends, M. Biczysko, T. Bligaard, C. H. Christensen, D. Clary, S. Dahl, R. Van Harrevelt, K. Honkala and H. Jonsson, *The Journal of Physical Chemistry B*, 2006, **110**, 17719-17735.
(11) C. J. van der Ham, M. T. Koper and D. G. Hetterscheid, *Chemical Society reviews*, 2014, **43**, 5183-5191.
(12) R. Schlogl, *Angew Chem Int Ed Engl*, 2003, **42**, 2004-2008.
(13) T. Murakami, T. Nohira, T. Goto, Y. H. Ogata and Y. Ito, *Electrochimica Acta*, 2005, **50**, 5423-5426.
(14) J. G. Howalt, T. Bligaard, J. Rossmeisl and T. Vegge, *Physical chemistry chemical physics : PCCP*, 2013, **15**, 7785-7795.
(15) I. Dance, *Chemical Communications*, 1997, **2**, 165-166.
(16) T. H. Rod, B. Hammer and J. K. Nørskov, *Physical review letters*, 1999, **82**, 4054-4057.
(17) T. H. Rod and J. K. Nørskov, *Journal of the American Chemical Society*, 2000, **122**, 12751-12763.
(18) B. K. Burgess and D. J. Lowe, *Chemical Reviews*, 1996, **96**, 2983-3012.
(19) T. H. L. Rod, A.; Norskov, J. K., *Journal of Chemical Physics*, 2000, **112**.
(20) E. Skulason, T. Bligaard, S. Gudmundsdottir, F. Studt, J. Rossmeisl, F. Abild-Pedersen, T. Vegge, H. Jonsson and J. K. Norskov, *Physical chemistry chemical physics : PCCP*, 2012, **14**, 1235-1245.
(21) V. Kordali, G. Kyriacou and C. Lambrou, *Chemical Communications*, 2000, **17**, 1673-1674.
(22) R. Lan, J. T. Irvine and S. Tao, *Scientific reports*, 2013, **3**, 1145-1151.
(23) J. H. Montoya, C. Tsai, A. Vojvodic and J. K. Norskov, *ChemSusChem*, 2015, **8**, 2180-2186.
(24) E. Skulason, V. Tripkovic, M. E. Björketun, S. Gudmundsdottir, G. Karlberg, J. Rossmeisl, T. Bligaard, H. Jónsson and J. K. Nørskov, *The Journal of Physical Chemistry C*, 2010, **114**, 18182-18197.
(25) P. Mars and D. W. Van Krevelen, *Chemical Engineering Science*, 1954, **3**, 41-59.
(26) C. D. Zeinalipour-Yazdi, J. S. Hargreaves and C. R. A. Catlow, *The Journal of Physical Chemistry C*, 2015, **119**, 28368-28376.
(27) Y. Abghoui, A. L. Garden, V. F. Hlynsson, S. Björgvinsdóttir, H. Ólafsdóttir and E. Skúlason, *Physical Chemistry Chemical Physics*, 2015, **17**, 4909-4918.
(28) Y. Abghoui and E. Skúlason, *The Journal of Physical Chemistry C*, 2017, **121**, 24036-24045.
(29) Y. Abghoui and E. Skúlason, *Catalysis Today*, 2017, **286**, 78-84.
(30) Y. Abghoui, A. L. Garden, J. G. Howalt, T. Vegge and E. Skulason, *ACS Catalysis*, 2015, **6**, 635-646.
(31) J. G. Howalt and T. Vegge, *Physical Chemistry Chemical Physics*, 2013, **15**, 20957-20965.
(32) D. V. S. Yandulov, R. R., *Science*, 2003, **301**, 76-78.
(33) D. V. S. Yandulov, R. R., *Journal of the American Society*, 2002, **124**, 6252-6253.

(34) D. V. S. Yandulov, R. R., *inorganic chemistry*, 2005, **44**, 1103-1117.
(35) R. R. Schrock, *Accounts of Chemical Reseach*, 2005, **38**, 955-962.
(36) R. R. Schrock, *Angew Chem Int Ed Engl*, 2008, **47**, 5512-5122.
(37) F. Neese, *Angew Chem Int Ed Engl*, 2005, **45**, 196-199.
(38) A. R. Singh, B. A. Rohr, J. A. Schwalbe, M. Cargnello, K. Chan, T. F. Jaramillo, I. Chorkendorff and J. K. Nørskov, *ACS Catalysis*, 2017, **7**, 706-709.
(39) P. Giannozzi, S. Baroni, N. Bonini, M. Calandra, R. Car, C. Cavazzoni, D. Ceresoli, G. L. Chiarotti, M. Cococcioni, I. Dabo, A. Dal Corso, S. de Gironcoli, S. Fabris, G. Fratesi, R. Gebauer, U. Gerstmann, C. Gougoussis, A. Kokalj, M. Lazzeri, L. Martin-Samos, N. Marzari, F. Mauri, R. Mazzarello, S. Paolini, A. Pasquarello, L. Paulatto, C. Sbraccia, S. Scandolo, G. Sclauzero, A. P. Seitsonen, A. Smogunov, P. Umari and R. M. Wentzcovitch, *Journal of physics. Condensed matter : an Institute of Physics journal*, 2009, **21**, 395502-395522.
(40) S. R. Bahn and K. W. Jacobsen, *Computing in Science & Engineering*, 2002, **4**, 56-66.
(41) J. Wellendorff, K. T. Lundgaard, A. Møgelhøj, V. Petzold, D. D. Landis, J. K. Nørskov, T. Bligaard and K. W. Jacobsen, *Physical Review B*, 2012, **85**, 235149-235171.
(42) J. Wellendorff, T. L. Silbaugh, D. Garcia-Pintos, J. K. Nørskov, T. Bligaard, F. Studt and C. T. Campbell, *Surface Science*, 2015, **640**, 36-44.
(43) H. J. Monkhorst and J. D. Pack, *Physical Review B*, 1976, **13**, 5188-5192.
(44) M. Volmer and T. Erdey-Gruz, *Principles of Adsorption and Reaction on Solid Surfaces*, Wiley-Interscience: Hoboken, NJ, USA, 1930.
(45) J. Heyrovský, *Recueil des Travaux Chimiques des Pays-Bas*, 1927, **46**, 582-585.
(46) G. Henkelman, B. P. Uberuaga and H. Jónsson, *The Journal of Chemical Physics*, 2000, **113**, 9901-9904.
(47) J. Tafel, *Z. Phys. Chem*, 1905, **50**, 641.
(48) J. K. R. Norskov, J.; Logadottir, A.; Lindqvist, L., *The Journal of Physical Chemistry B*, 2004, **108**, 17886-17892.
(49) E. Skulason, G. S. Karlberg, J. Rossmeisl, T. Bligaard, J. Greeley, H. Jonsson and J. K. Norskov, *Physical chemistry chemical physics : PCCP*, 2007, **9**, 3241-3250.
(50) S. A. Wasileski and M. J. Janik, *Physical chemistry chemical physics : PCCP*, 2008, **10**, 3613-3627.
(51) J. Rossmeisl, E. Skúlason, M. E. Björketun, V. Tripkovic and J. K. Nørskov, *Chemical Physics Letters*, 2008, **466**, 68-71.
(52) K. Chan and J. K. Norskov, *The journal of physical chemistry letters*, 2015, **6**, 2663-2668.
(53) G. Henkelman, A. Arnaldsson and H. Jónsson, *Computational Materials Science*, 2006, **36**, 354-360.
(54) J. K. Norskov, F. Studt, F. Abild-Pedersen and T. Bligaard, *Fundamental concepts in heterogeneous catalysis*, John Wiley & Sons, 2014.
(55) X. Liu, J. Xiao, H. Peng, X. Hong, K. Chan and J. K. Norskov, *Nature communications*, 2017, **8**, 15438-15444.
(56) A. Logadottir, T. H. Rod, J. K. Nørskov, B. Hammer, S. Dahl and C. J. H. Jacobsen, *Journal of Catalysis*, 2001, **197**, 229-231.
(57) F. Abild-Pedersen, J. Greeley, F. Studt, J. Rossmeisl, T. R. Munter, P. G. Moses, E. Skulason, T. Bligaard and J. K. Norskov, *Phys Rev Lett*, 2007, **99**, 016105-016108.
(58) L. D. Chen, M. Urushihara, K. Chan and J. K. Nørskov, *ACS Catalysis*, 2016, **6**,

7133-7139.